Journal of Applied Polymer Science

A Simple, Inexpensive, Real-Time Interferometric Cure Monitoring System for Optically Cured Polymers

Robert E. Schwerzel,[1] Amit S. Jariwala,[1,2] David W. Rosen[2]

[1]AlpZhi Inc., Atlanta, Georgia 30318

[2]George W. Woodruff School of Mechanical Engineering, Georgia Institute of Technology, Atlanta, Georgia 30332

Correspondence to: R. E. Schwerzel (E-mail: bobs@alpzhi.com)

ABSTRACT: Optically cured polymers play a crucial role in many commercial applications, ranging from UV-cured inks, coatings, and dental fillings to the optical fabrication of three-dimensional prototypes by means of stereolithography. However, our understanding of the detailed processes that occur in the curing of these materials is often limited by the practical difficulty of observing the cure process in real time, under "real-world" conditions. This article reports the simple implementation of a free-space Mach-Zehnder interferometer that can be constructed inexpensively from readily available components, and demonstrates its utility in monitoring the UV curing of a typical acrylate photopolymer system in real time. In particular, it is shown that this system can sensitively track the induction period, the light-induced photopolymerization reaction, and the subsequent dark reaction that continues after the irradiation has been halted. This Interferometric Cure Monitor, or "ICM," thus provides a valuable addition to other analytical methods, both for improving the quality control of existing commercial processes and for aiding the development of improved photopolymer formulations. © 2013 Wiley Periodicals, Inc. J. Appl. Polym. Sci. 129: 2653–2662, 2013

KEYWORDS: photopolymerization; optical properties; photorefractive effects; kinetics; crosslinking

Received 18 April 2012; accepted 31 December 2012; published online 30 January 2013

DOI: 10.1002/app.38993

INTRODUCTION

It is well established that photopolymerization reactions can lead to substantial increases in refractive index, and that in the absence of other additives these increases result primarily from the densification that occurs as individual monomer molecules are "zipped" together to form either linear or branched polymer networks, depending on the monomers used.[1] This phenomenon is responsible for the long-standing interest in photopolymerization for applications in optical waveguide fabrication,[1] holographic data storage,[1–3] and the fabrication of three-dimensional optical elements.[4–6] It has also spurred the use of optical interference techniques, such as holography[7,8] or interferometry,[9–14] as tools for studying the photopolymerization process in real time.

In this article, a simple real-time monitoring system based on Mach-Zehnder interferometry is presented that enables one to monitor the extent of curing in a photopolymer process. This Interferometric Cure Monitor, or "ICM," system provides real-time information about the dynamics of the photopolymerization phenomena, and it provides the foundation for future real-time feedback control systems currently under development in our laboratories.

Previous researchers have typically employed either Michelson[11,12] or Mach-Zehnder[13,14] interferometer configurations in their studies of photopolymerization reactions. However, these prior schemes have used elaborate, delicate optical systems with multiple mirrors and beam-splitters, making them expensive and time-consuming to set up. In contrast, by using the reflections from the front and back surfaces of the sample cell itself as the basis of our interferometer, we have been able to obtain comparable results with excellent signal-to-noise ratios in a simple, robust configuration.

The primary operational distinction between the two types of interferometers is that a Michelson interferometer utilizes the same beam splitter to both separate a laser beam into sample and reference beams and then recombine the beams to create the interference pattern and direct the resulting light into a detector, while a Mach-Zehnder interferometer typically utilizes a beam splitter to separate the sample and reference beams but then recombines the beams downstream of the sample, lending itself to a more linear design. For example, integrated-optic Mach-Zehnder interferometers are commonly employed as electrooptic modulators to convert electrical signals to optical pulses in fiber-optic telecommunications systems.[15]

In our case, the front surface of the sample cell acts as both the upstream beam splitter and downstream combiner, with the front-surface reflection providing the reference beam and the reflection from the back of the sample cell (which has made a round-trip passage through the reactive photopolymer material) providing the sample beam. Interference between these two reflected beams contains a wealth of useful information about the chemical and physical changes occurring within the photopolymer before, during, and after its photo-induced curing reactions, as described in detail below.

EXPERIMENTAL

Irradiation Apparatus

In the present work, an Omnicure® S2000 UV spot curing system from Lumen Dynamics was used for all irradiations. This system consists of a high-pressure 200-Watt mercury vapor short arc lamp coupled to a 5 mm UV-transmitting light guide. Broad-band UV light from the lamp was conditioned by passing it through a narrow-band 365 nm interference filter, a collimating lens, and a ground glass diffuser (obtained from Thorlabs, Inc.). The resulting spatially homogenized light was then directed onto a Texas Instruments' Digital Micromirror Device (DMD™) by means of a UV-coated front-surface mirror.

The DMD™ is an array of individually addressable, bistable micromirrors that can be selectively oriented to display any desired bitmap, with each pixel of the bitmap controlling one and only one micromirror on the DMD™. With the appropriate design of either binary (black/white) or gray-scale bitmaps, any desired image can be projected from the DMD™ onto the photocurable resin. In the present system, the DMD™ is positioned beneath the sample chamber, so the photocurable resin is cured from the bottom up. In previous (unpublished) work, however, an inverse system has been used, with UV light from a light guide delivered to the resin sample from above. The ICM system can be configured to work equally well in either orientation. A simple objective lens is used reduce the size of the image projected by the DMD™ into the resin sample by about half, such that the cured shapes have a maximum length of about a centimeter. In practice, the cured shapes are typically much smaller than this, with sizes on the order of a millimeter or two. The shiny frame of the DMD™ is left unmasked, so it always reflects UV light into the resin regardless of the bitmap being projected, and thus provides a constant reference frame around the shape (or shapes) being cured. The sample cell is supported by a rigid horizontal stage having an opening for the UV light to pass through, and one end of the cell is gripped by a custom-made holder attached to an X-Y translation stage so the cell can be moved both sideways and front-to-back on the support stage. This allows up to 16 individual exposures to be made in a single cell, so many different experiments can be carried out quickly and easily.

Interferometric Cure Monitoring System

The ICM system described here uses the sample cell itself as the basis for a free-space Mach-Zehnder interferometer. The sample cell consists of two glass microscope slides held closely together with a spacer of known thickness placed along two edges, as shown schematically in Figure 1. The lower slide acts as a substrate upon which the resin composition is cured, while the upper slide serves to provide a smooth, flat window for the laser beam of the ICM system.

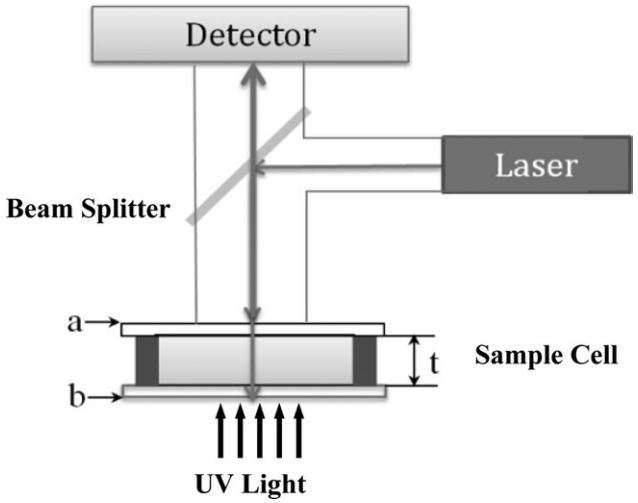

Figure 1. Schematic illustration of the ICM system.

A coherent beam from a low-power red diode laser (670 nm, Thorlabs, Inc.) is directed by a beam splitter (Thorlabs, Inc.) at right angles into the sample cell containing a photopolymer resin that is transparent at the wavelength of the laser and has a physical thickness *t*. Interference occurs between the light reflecting from the front surface of the sample cell (a) and the light reflecting from the back surface of the cell (b) as shown schematically in Figure 1. Because UV irradiation causes polymerization and densification of the resin, the refractive index of the material in the irradiated regions increases as the density of the resin increases during polymerization; the intensity of the reflected laser beam therefore exhibits a periodic modulation of maxima and minima as the front-surface and back-surface reflections go in and out of phase with one another.

For our initial feasibility studies of the ICM concept, the detector consisted of a simple module incorporating a Texas Instruments' OPT-101P photodetector chip, wired in accordance with Texas Instruments' standard guidelines for this chip and powered by an off-the-shelf 12V DC power supply from Radio Shack. The OPT-101P chip includes built-in circuitry that enables it to provide a linear voltage output in response to changes in the detected light intensity, making it ideal for our purposes. The detector chip and its associated circuitry were mounted in a small opaque plastic project enclosure box, also from Radio Shack. A 1/4-inch hole was drilled in one face of the box to serve as a window for the laser beam, and was covered with a small piece of red plastic camera filter (Cokin, obtained from a local camera store) to prevent stray room light from reaching the detector chip. The output voltage from the chip was coupled to a lab computer via a National Instruments A-to-D module, and was displayed using LabView software. Initial experiments with the irradiation of the simple photocurable acrylic resin described below showed that this system was capable of producing real-time interference fringes with excellent signal-to-noise ratios; the data presented in Figures 3 to 9 were obtained using this system.

While this early ICM system was a single-beam apparatus in which the laser beam interrogated only a portion of the region of the sample undergoing photopolymerization, it would be a simple extension of the system to incorporate a second, reference beam that could monitor a spot on the sample away from the irradiation zone. The output from this reference interferometer could then be electronically subtracted from the output of the photopolymerization interferometer to give a compensated signal that automatically zeroed out any variations resulting from temperature changes, shrinkage or expansion of the sample cell, and so on. The output from the reference detector could also be monitored directly to provide a measure of, for example, whether shrinkage was changing the physical path length of the sample cell t to a significant extent.[12]

In view of this objective, the capabilities of the ICM were recently upgraded to enable this type of measurement and more by replacing the simple detector module with a small digital video camera (Basler Ace acA2500-14gm, 5MP CMOS, obtained from Graftek Imaging). A user interface for decoding the camera data was developed in LabView; this allows the user to save the live video file as an .avi file and to display the time evolution of the intensity variation of any given pixel either in real time during the irradiation or later, in playback mode. In addition, a 10× beam expander and a variable iris aperture mounted on an X-Y translation stage (all obtained from Thorlabs, Inc.) were mounted between the diode laser and the beam splitter. This arrangement allows the complex interference patterns that develop across the entire region illuminated by the DMD™ to be monitored in real time by opening the aperture fully, and makes it possible to observe the formation of the cured part directly as its image emerges from the interference patterns across the sample; we refer to this configuration as "full-aperture ICM." Alternatively, the aperture can be closed down to select only a small portion of the expanded laser beam, and this small beam can be directed to any desired portion of the irradiated area by moving the aperture with the X-Y translation stage. We refer to this configuration as "small-aperture ICM." In addition, because the software associated with the video camera allows any individual pixel within the image area to be selected and displayed over time, the evolution of the interference pattern for any part of the sample can be monitored, as we have previously reported in part.[16]

In practice, when using a shaped bitmap to cure only a portion of the region covered by the DMD™ image, it is useful to use full-aperture ICM to visualize exactly where the polymerized shape appears within the frame and to select a pixel within the cured region; the sample chamber can then be translated to bring a fresh portion of resin into the beam from the DMD™, the aperture can be closed down to a small beam which is positioned over the selected pixel, and the irradiation repeated with the time evolution of the fringes monitored by the video camera. Figures 10 and 11 show excellent examples of the information provided by this approach.

We note that the beam splitter and the normal incidence geometry that we have employed were adopted solely for convenience in adapting our current irradiation apparatus, which is built around a Thorlabs' cage framework system, to accommodate the ICM; the experimental results we obtained, and the analysis principles described below, would be the same if the laser and detector were mounted symmetrically off-axis to each other with no incident beam-splitter, provided only that the angle of incidence (measured from the normal) for both the laser and the detector was small, typically less than 10° or so. This geometry has been confirmed to work equally well in earlier, unpublished studies. We note also that an added benefit of this geometry (either normal or with a small angle of incidence) is that it renders the reflected intensities of the laser beams insensitive to polarization effects,[17] so the rotational orientation of the inherently polarized laser beam becomes unimportant.

Materials and Sample Handling

We used the tri-functional acrylate monomer trimethylolpropane triacrylate (TMPTA, SR-351) obtained from Sartomer and used as obtained, with 5% by weight of the photoinitiator 2,2-dimethoxy-1,2-diphenylethan-1-one (DMPA, Irgacure-651) used as obtained from BASF, as the resin composition. This composition exhibits greater than 90% transmission throughout the visible spectrum when completely cured. The actinic irradiance was controlled by directly setting the intensity levels on the light source power supply, and the exposure time was controlled by projecting a slide on the DMD™ for a specified amount of time through the options provided by Microsoft® PowerPoint®.

Following the irradiation, we used an aqueous surfactant solution to wash uncured resin from the samples, followed by removing any residual liquids with a gentle stream of nitrogen gas. The height of the cured parts was measured by three-dimensional non-contact confocal microscopy after a flood exposure with UV light had fully hardened the cured samples.

We wish to emphasize that we have intentionally left the inhibitors and dissolved oxygen in each sample of photopolymer resin. While this is perhaps contrary to traditional methods of studying photopolymerization kinetics, our ultimate objective is the fabrication of complex, precise plastic lenses and other optical components; and the inhibitors and oxygen aid significantly in the spatial confinement of the photopolymerization reaction by reducing the extent of dark reactions that would otherwise occur outside the irradiated region. We also note that the irradiations are typically carried out under conditions that result in cured parts having a thickness much less than the thickness of the sample cell; because the cured parts are small in size and never grow to reach the upper surface of the cell, each part is formed in an essentially infinite bath of resin, and bulk shrinkage of the cell is physically precluded (*vide infra*).

Working Principle

When a coherent laser beam is directed into a layer of sample material of thickness t that is transparent at the wavelength of the laser, interference can occur between the light reflecting from the front surface of the material (a) and the light reflecting from the back surface of the material (b), as shown schematically in Figure 2, provided that the angle of incidence of the beam (θ, measured from the normal) is sufficiently small (typically less than 10° or so) to provide good overlap between the incident and reflected beams.

Depending on the details of the experiment—the wavelength of the laser, the thickness of the material, the refractive index of the material at the wavelength of the laser, and the angle of incidence of the laser beam—this interference can be either constructive, leading to an increase in the intensity of the reflected beam, or destructive, leading to a decrease in the intensity of the reflected beam.

In practice, the situation is somewhat more complicated than this, as interference also occurs between the front-surface and back-surface reflections from the upper and lower glass windows. However, because these interferences do not change in response to changes in the material, they do not affect our measurements except to the extent that they impact the unchanging background intensity of the reflected laser beam. One additional complication comes into the analysis because the path of the laser beam is bent as it enters and exits the material, as shown in Figure 2. According to Snell's Law, the angles θ and θ′ are related to the refractive indices of air (n_1) and of the material (n_0) at the wavelength of the laser by

$$n_1 \sin\ \theta = n_0 \sin\ \theta' \tag{1}$$

so the round-trip optical path length of the light within the material (L) is given (for the case in which the angle of incidence of the laser beam is close to normal incidence) by

$$L = 2n_o l = 2n_o t/\cos\ \theta' = 2n_o t/\cos[\mathrm{a}\sin(n_1/n_0)\sin\theta] \tag{2}$$

where L is the total round-trip optical thickness of the sample, t is the physical thickness of the sample in μm, and l is the physical path length of the laser beam in the sample material (expressed in μm).

If the refractive index of the sample material changes during the measurement, as is expected for a photopolymer being irradiated, the resulting change in the optical thickness of the material is then given by

$$\Delta L = 2\Delta n l = 2(n_t - n_o)t/\cos\theta' \tag{3}$$

where n_o is the initial refractive index of the material and n_t is the refractive index of the material after exposure for a given period of time to UV light of a given wavelength distribution and intensity. From this, it can be seen that the change in the round-trip optical path length of the laser beam within a photocurable resin material during a photopolymerization process will be given by

$$\Delta L = 2\Delta n t/\cos\theta' = 2\Delta n t/\cos[\mathrm{a}\sin(n_1/n_0)\sin\theta] \tag{4}$$

or, taking n_1 to be the index of air, ~1.000 and $n_0 = 1.4723$ for our sample photopolymer,[18] with $\theta = 10^\circ$ for purposes of illustration, we get

$$\Delta L = 2\Delta n t/\cos[\mathrm{a}\sin(n_1/n_0)\sin\theta] = 2\Delta n t/\cos 7.4^\circ = 2.017\Delta n t \tag{5}$$

Thus, for typical acrylate photopolymer materials with values of $\mathbf{n_0}$ in the range of 1.4 to 1.5, and for ICM geometries having θ less than around 10°, we can simply say as an acceptably good approximation that

$$\Delta L \approx 2\Delta n t \tag{6}$$

The maximum change in the intensity of the reflected beam will occur when the change in the round-trip optical path length of the laser beam within the material (ΔL) is equivalent to one-half of the wavelength of the laser light, λ, as this has the effect of shifting the wave crests of the light waves reflected from the front and back surfaces of the material from being in-phase to out-of-phase, or *vice versa*. This can be expressed as a fraction of the laser wavelength, or the Wave Shift, by

$$\text{Wave Shift} = \Delta L/\lambda \tag{7}$$

For our purposes, the initial direction of the intensity change (increase vs. decrease) is unimportant, since each measurement starts at a completely arbitrary reflected intensity and we have no control over the initial interference condition of the front-surface and back-surface reflected laser beams. However, we note that changes in the direction of the intensity change (that is, phase reversals) that occur during a measurement are nonetheless quite informative, as they can signal a change in process from photochemical cure (typically resulting in shrinkage) to thermal expansion due to warming of the material, or from photochemical cure to thermal dark reaction after the light has been turned off.

The overall intensity of the reflected laser beam follows a cosine curve as a function of the Wave Shift, with a maximum intensity when the wave crests of the electric field vectors of the front-surface reflection match up with the wave crests of the electric field vectors of the back-surface reflection, and minimum intensity when the two sets of wave crests are exactly out of phase with one another. It is therefore more useful to express the Wave Shift of eq. (7) as a Phase Shift, Ø, with units of 2π radians of phase difference between the wave crests of the two beams.

$$\varnothing(\text{radians}) = 2\pi\Delta L/\lambda = 2\pi(2\Delta n t)/\lambda = 4\pi\Delta n t/\lambda \tag{8}$$

In general, for any arbitrary phase shift Ø, the refractive index change responsible for the phase shift will therefore be given by:

$$\Delta n = \lambda\varnothing/4\pi t \tag{9}$$

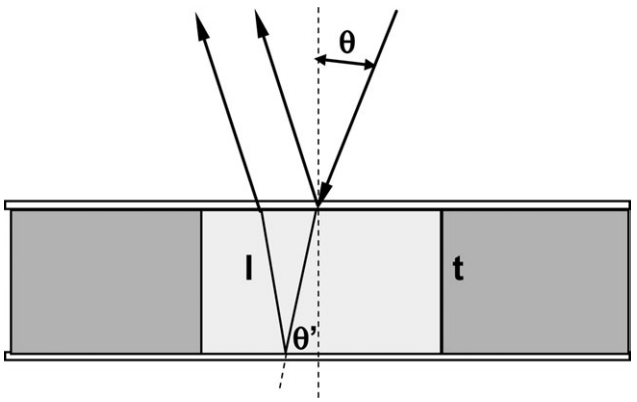

Figure 2. Schematic optical paths through the sample cell.

and for the specific case where $\lambda = 0.670$ microns (for our typical red diode laser),

$$\Delta n = 0.053 \varnothing / t \quad (10)$$

We thus find a linear relationship between the total phase shift and the change in the refractive index that occurs during the reaction. Because the photopolymer curing reaction propagates vertically through the resin sample as the irradiation proceeds, the change in refractive index is tied directly to the height of the cured polymer within the resin sample. Thus, the observed phase shift is also a direct measure of the height of the cured region of polymer as the reaction proceeds. We note that this analysis assumes that the physical thickness of the sample chamber does not change during the irradiation, which is appropriate given the rigidity of the glass microscope slides used to form the sample chamber and the small area (typically less than 1–2 mm^2) of the photopolymer that is irradiated in any given experiment. This assumption has been verified experimentally, as will be described below.

RESULTS AND DISCUSSION

A representative example of the data provided by the ICM system is shown below in Figure 3 for irradiation of a 250-micron thick sample of photopolymer resin at 20 W/cm^2, with the detector output plotted against time in seconds. A number of salient features are evident from the figure. An induction period is clearly visible at the left side of the trace as dissolved oxygen and inhibitors in the photoinitiator are scavenged before the polymerization process can get underway. Then, toward the right side of the trace, a continuing densification that we ascribe to thermal dark reaction is apparent after the irradiation has stopped, followed by eventual equilibration. About 27.5 full oscillations of the intensity, or interference fringes, are visible, corresponding to a total phase shift of approximately 173 radians. These fringes are the result of the changes in both the density and the height of the part cured within the layer of resin.

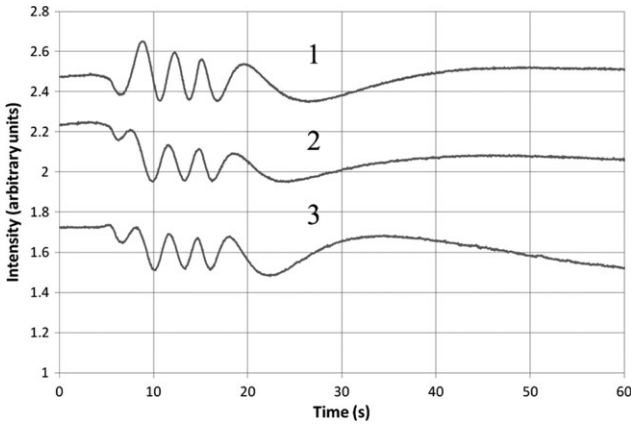

Figure 4. Consistent kinetics from three consecutive experiments.

To demonstrate the reproducibility of the interferometric measurements, three separate 250-micron thick samples were cured with identical exposures and irradiance. The results from the three experiments are shown in Figure 4.

We note that the charts are plotted in arbitrary units for the intensity of the reflected laser beam, so only the number of fringes is of importance (the three curves differ somewhat in shape because of differences in the initial phase relationship between the front and back reflections from sample to sample). The key result is that all three samples yielded essentially the same number of fringes (~4 1/2), and therefore the same total phase shift ($\varnothing \approx 9\pi$ radians) and the same overall change in refractive index, over the course of the reaction. The final height of each cured part was measured by confocal microscopy to be approximately 122 microns.

The ICM system also helps in visualizing the effect of total UV exposure (by varying the exposure time at a fixed constant irradiance) on the initiation of polymerization, as shown in Figure 5. Different 250-micron thick samples were exposed at a constant irradiance of 20 W/cm^2 for times varying by

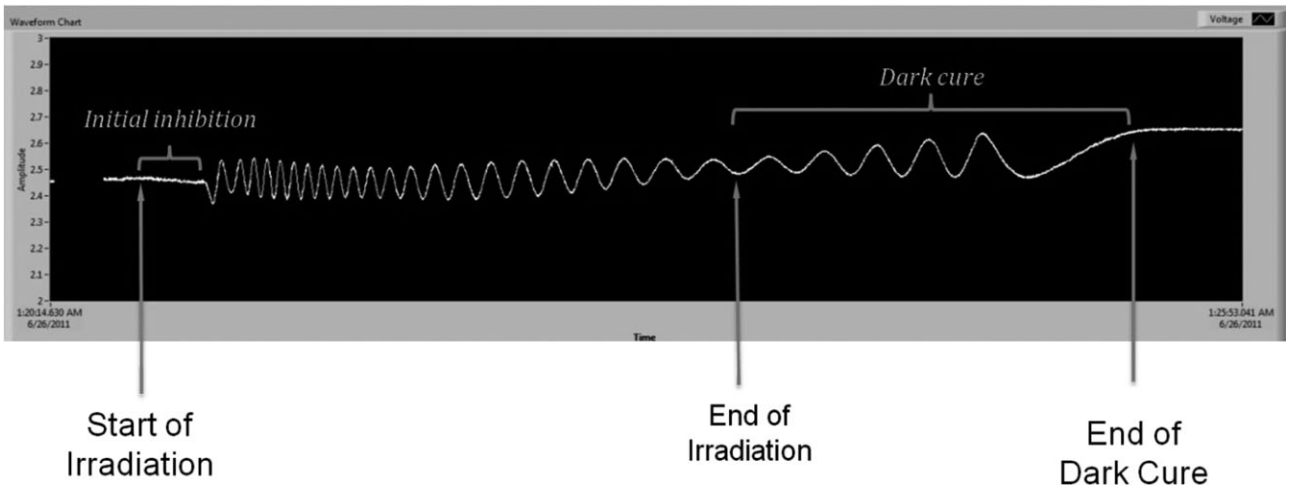

Figure 3. ICM results for curing a 250-micron thick sample of resin.

Applied Polymer SCIENCE

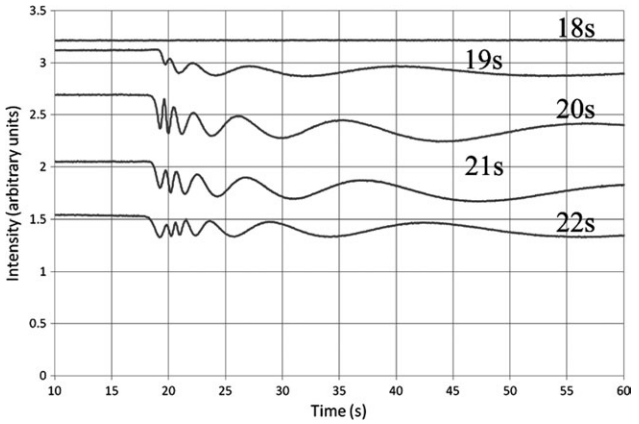

Figure 5. Effect of varying total exposure dose (by varying the exposure time).

increments of 1 s on either side of the observed photoinitation period of ~19 s under these conditions.

It can be seen that no photopolymer forms with only 18 s of exposure, as some of the inhibitors and/or dissolved oxygen still remain in the resin at this point; the reaction only begins with 19 s of exposure and proceeds progressively with increased exposure time. The number of fringes increases with increasing total exposure dose, as a result of the increased densification of the irradiated region as the height of the cured part increases with increasing exposure. We note that because the exposure times are all quite short relative to the overall time span of each experiment, nearly as many fringes result from dark reaction as from the immediate photopolymerization during the exposure itself. We also note that the slow-down of the dark reaction, as residual free radicals in the resin eventually find each other and react to form new bonds, is evident from the curves; while some of the residual radicals may be scavenged by traces of inhibitor or oxygen, these processes do not lead to changes in refractive index, as evidenced by the absence of fringes during the indution period at the beginning of each irradiation.

One of our primary objectives in developing the ICM system was to assist in estimation of the height of the cured part during an irradiation in real time. Figure 6 shows the correlation that was observed between the height of a samples cured using a rectangular shaped bitmap, as measured by confocal microscopy, and the corresponding total phase angle.

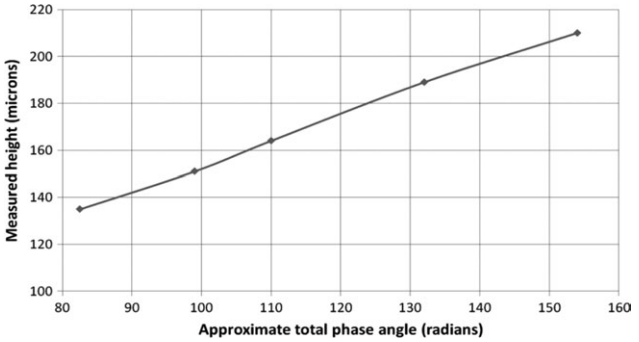

Figure 6. Correlation between cured sample height and total phase angle.

The dots in Figure 6 represent actual experimental data points. Each final cured part was washed in an aqueous surfactant solution and post-cured by flood exposure with 365 nm light prior to measuring its height; we ascribe the slight deviations observed to variations in the shape of the cured part introduced by the washing procedure (which is still being optimized) before flood cure, since the surface of the cured part is initially a soft gel of partially cross-linked oligomers.

Figure 7 shows a confocal microscope image of the rectangular cured sample that was used for Figure 6. This sample was fabricated by projecting a uniformly illuminated square PowerPoint® bitmap into the resin, and this uniformity is reflected in the shape and profile of the cured sample. We have frequently used this image and others like it in our experiments, as these images provide a sensitive test of the alignment and focus of the optical system.

In order to further explore the utility of the monitoring system, we conducted a number of experiments to highlight the effects of chemical inhibition (caused by dissolved oxygen and inhibitors) on photopolymerization. Specifically, we conducted several experiments by varying the spacer thickness (and thus the thickness of the sample cell, t), as shown in Figure 8. The two plots were obtained from two different experiments, where the samples were irradiated with the same irradiance (25 W/cm^2) for 25 s.

Essentially no curing was observed when a thicker spacer (1.4 mm) was used, whereas the same resin was cured easily to a height of 106 μm with a thinner, 200-μm spacer. We ascribe this effect to continued inhibition of the photopolymerization reaction by rapid diffusion of dissolved oxygen into the irradiation zone from the larger reservoir of air-saturated resin in the thicker sample. As shown by the previous results in Figure 5 for a 250-micron sample, a 25-s exposure at this irradiance should have been more than sufficient to cause a significant amount of photopolymerization to occur, were it not for the rapid diffusion of dissolved oxygen; while dissolved inhibitors are also present in the reservoir of unreacted resin, these molecules are relatively large, and their diffusion is correspondingly slow, compared to that of molecular oxygen.

Another interesting result obtained with the ICM system was the effect of irradiation intensity on the course of the photopolymerization reaction, as shown in Figure 9.

Four experiments were conducted by providing the same total exposure (800 μJ/cm^2) but varying the irradiance from 20 μW/cm^2 with a 40 s exposure to 200 μW/cm^2 with a 4 s exposure (increasing from top to bottom). The initial photoinitiation period was progressively reduced with higher exposure intensities, as expected from the reaction kinetics; the greater the light intensity, the greater the rate of free radical formation from the photoinitiator, so dissolved oxygen and other inhibitors are scavenged more rapidly and the photopolymerization reaction can then proceed more quickly. The ICM provides a direct window into the details of this process, in real time.

It is evident in all of the experiments discussed above that the rate of polymerization decreases continuously both during and after irradiation, and this observation merits further discussion.

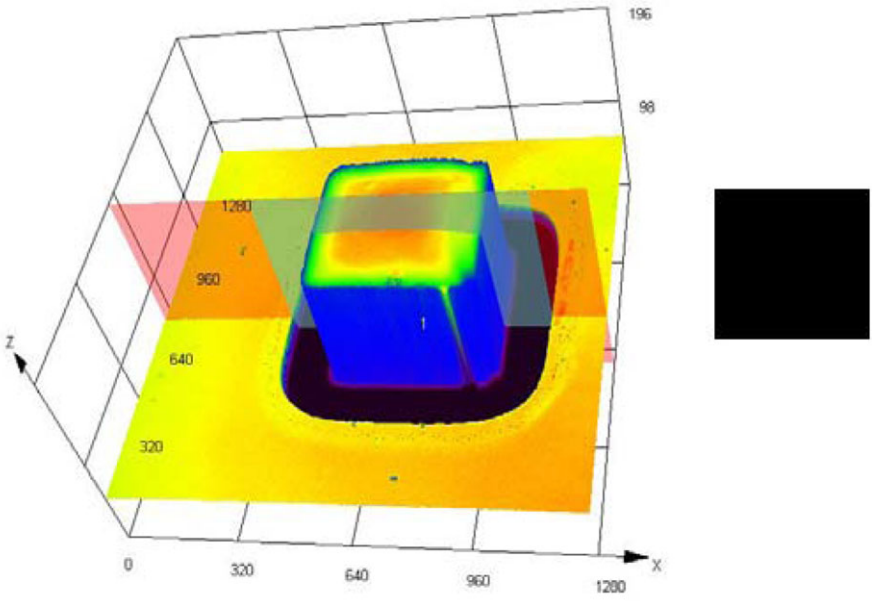

Figure 7. Confocal microscope image of a representative cured sample, showing the PowerPoint® bitmap used for this irradiation. [Color figure can be viewed in the online issue, which is available at wileyonlinelibrary.com.]

We consider that two different factors are responsible for this behavior. First, because the Irgacure 651 photoinitiator (a benzoin ether initiator) necessarily absorbs light at our irradiation wavelength of 365 nm, the intensity of the light decreases exponentially according to the Beer-Lambert Law as it propagates upward through the sample cell. This means that the rate of radical formation, and thus the ability of the photopolymerization process to compete with radical scavenging by the inhibitors and dissolved oxygen, also varies exponentially through the thickness of the sample cell. This factor does not change appreciably during the course of the reaction, as the byproducts from the fragmentation of benzoin ethers also have absorbance at 365 nm[19,20] and hence continue to attenuate the light as a function of distance through the cell. This is explicitly accounted for in the design of the irradiation profile for each individual shape to be made, including both the shape and size of the bitmap (or bitmaps) to be used and the time that the bitmap(s) will be projected from the DMD™.

The second factor is simply the progressive increase in viscosity, and the corresponding decrease in mobility and diffusion rates, that occurs as the polymerization reaction progresses.[9–11] Even in an infinitesimally thin layer of resin for which Beer-Lambert effects would be negligible, it is to be expected that the reaction would slow down and eventually stop as the individual monomer molecules formed longer and longer chains and/or branches and the reactive radicals on the ends of these chains eventually reacted either with other radicals or with scavengers such as oxygen. This effect is also taken into explicit account by incorporating our best estimates of reaction rates and diffusion constants into the design of the irradiation profile for each desired shape.

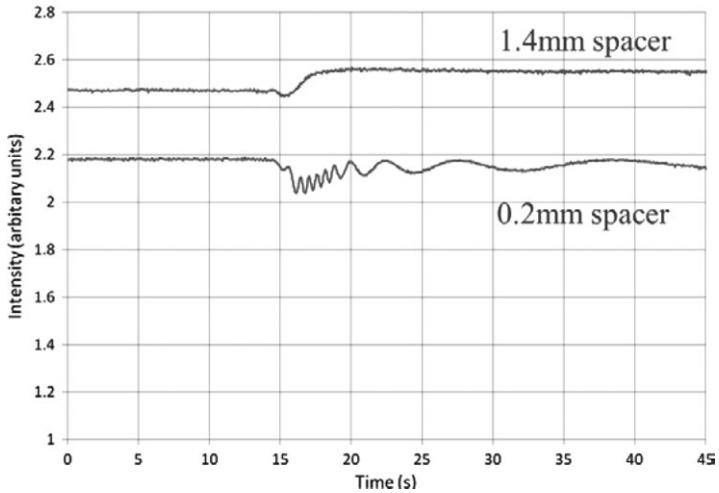

Figure 8. Effect of varying the sample cell thickness on photopolymerization.

Applied Polymer SCIENCE

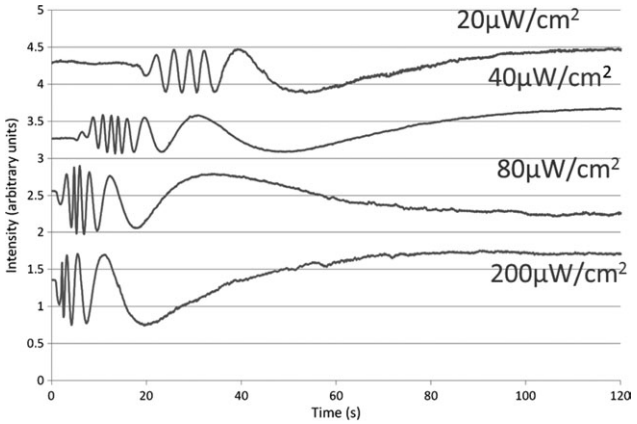

Figure 9. Effect of varying irradiance (total exposure dose kept constant).

Finally, a series of experiments were carried out using the upgraded ICM system (with the video camera and variable aperture as described previously) to confirm that the fringe patterns we observe are in fact due solely to the growth of photopolymer in the irradiated region and not to other reactions or bulk shrinkage of the sample cell. These results are shown in Figures 10 and 11.

First, a square bitmap was projected into a 250-micron thick sample, with the bitmap centered in the DMD™ frame as shown in Figure 10(A), and irradiated at low irradiance for 300 s; this was sufficient to cure the sample to a height of approximately 120 microns, or roughly halfway through the thickness of the cell. With the aperture of the ICM laser fully open, so the beam covered the entire frame of the irradiated area, the interference pattern shown in Figure 10(B) was observed at the conclusion of the irradiation. This interference pattern is rather complex, and requires some explanation. The key feature is the nominally square "hump" surrounded by circular fringes in the center of the frame; this is the interference image of the actual cured shape immediately after the irradiation, and it can be seen to grow in while the irradiation is in progress. The other, larger circular patterns, and the bold diagonal linear fringes, result from the microscope slides that comprise the sample cell. We have observed that these features will appear even in the full-aperture ICM image of a single fresh microscope slide, due to variations in the thickness of the slide on the scale of the wavelength of light. We also note that while full-aperture ICM is very useful for visualizing the formation of the complete shape in real time, the analysis of the fringe patterns produced is difficult, as different parts of the expanded laser beam can be refracted at various angles by the growing polymer shape and will thus interfere in complex ways with the incoming light.

For this reason, to monitor the time evolution of the growing part, we chose a single pixel in the center of the frame [indicated by the arrow in Figure 10(B)], moved the cell laterally to expose a fresh region of resin, and repeated the irradiation with the ICM aperture closed down to produce a laser spot only a few millimeters in diameter. This produced the clean fringe pattern shown in Figure 10(C), clearly reflecting the growth of the polymer as a function of irradiation time.

The same cell was then translated again to expose a fresh region of resin, the ICM aperture was again opened fully, and the irradiation was carried out exactly as before but with a new bitmap that was positioned off-center, as shown in Figure 11(A,B). (With the configuration of our optical system, the DMD™ chip inverts the image as it is projected into the sample cell, so the square at upper left in the bitmap results in curing a square at lower left in the resin.)

The cell was then again translated laterally, the ICM aperture was again closed down without moving the laser beam from the

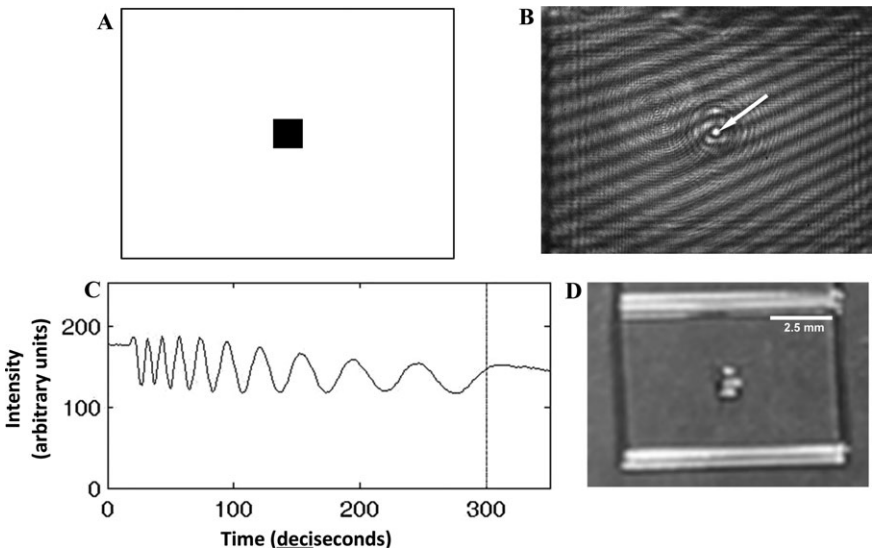

Figure 10. ICM monitoring of centered bitmap photopolymerization. (A) Bitmap and DMD™ frame; (B) full-aperture ICM image showing cured shape in center and location of center pixel monitored for time evolution of polymerization (arrow); (C) time evolution of small-aperture interference pattern at center pixel during center photopolymerization; (D) photograph of polymerized shape after washing and flood-cure.

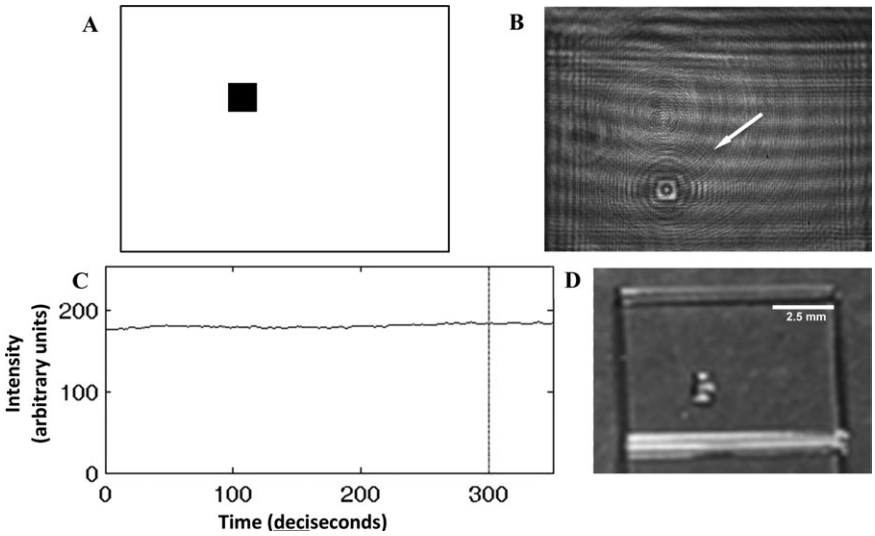

Figure 11. ICM monitoring of off-center bitmap photopolymerization. (A) Bitmap and DMD™ frame; (B) full-aperture ICM image showing cured shape at lower left and location of center pixel monitored for time evolution of polymerization (arrow); (C) time evolution of small-aperture interference pattern at center pixel during off-center photopolymerization; (D) photograph of polymerized shape after washing and flood-cure.

center of the sample, and the off-center bitmap irradiation was again carried out while we monitored the same center pixel that had been used before [at the arrow in Figure 11(B)]. Even though the irradiation clearly results in polymerization, as shown by Figure 11(B,C) shows that no fringes whatsoever appear in the center of the frame, only a few millimeters away. This demonstrates convincingly that in our system, under our conditions, there is no bulk shrinkage of the resin in the sample cell, and that the interference fringes we observe result only from the growth of polymer in the irradiated regions.

Finally, the cell was dismantled, unreacted resin was removed by washing, and the cured shapes were subjected to an overall flood cure at 365 nm to fully harden them. The center and off-center shapes are shown in Figures 10(D) and 11(D), respectively (the cured parts are difficult to photograph because of their transparency, and are shown here at an oblique angle that unfortunately also shows some reflections from their tops and sides). The salient point is that these photographs show clearly that polymer has been formed exactly where the full-aperture ICM images show that curing has occurred, and that interference fringes develop over time only in the regions where polymerization is occurring and nowhere else in the frame of the DMD™.

SUMMARY AND CONCLUSIONS

The work presented here shows that a simple, robust interference cure monitoring system, built around a simple sample cell configuration, can be used to estimate the height of a cured photopolymer part in real time during the irradiation, that it can provide valuable insights into the effects of dissolved oxygen on the initiation and progression of the photopolymerization reaction, and that it can monitor the progress of the dark polymerization reaction that continues for some time after the irradiation has been stopped as residual reactive "living polymer" radicals are gradually scavenged or otherwise terminated. With the addition of a beam expander and variable aperture, it gains the ability to visualize directly the formation of a photopolymer shape in real time.

The fact that interference fringes are observed only when and where the cured photopolymer shape is being formed, and not in other regions of the cell (nor even in the irradiated region during the initiation period when dissolved oxygen and inhibitors are being scavenged) demonstrates convincingly that photopolymerization is the only process being monitored in our experiments. The ICM system described here can be further improved to provide real-time, closed-loop feedback control of the photopolymerization process, thus improving the overall accuracy and reproducibility of the parts being cured; work directed toward this end is currently in progress in our laboratories.

ACKNOWLEDGMENTS

This article is based upon work supported by the National Science Foundation under Grant No. SBIR IIP 1047095. The authors are also thankful to the support provided by a Georgia Research Alliance VentureLab grant for technology commercialization. This work was previously presented in part at the Twenty-Second Annual International Solid Freeform Fabrication (SFF) Symposium—An Additive Manufacturing Conference, held at The University of Texas in Austin on August 8-10, 2011.[21]

REFERENCES

1. Tomlinson, W. J.; Chandross, E. A. *Adv. Photochem.* **1980**, *12*, 201.
2. Dhar, L.; Hale, A.; Katz, H. E.; Schilling, M. L.; Schnoes, M. G.; Schilling, F. C. *Opt. Lett.* **1999**, *24*, 487.

3. Gleeson, M. R.; Liu, S.; Sheridan, J. T. *J. Mater. Sci.* **2009**, *44*, 6090.
4. Streppel, U.; Dannberg, P.; Waechter, C.; Michealis, D.; Kowarschik, R.; Braeuer, A. *Proc. SPIE* **2003**, *4991*, 321.
5. O'Neill, F. T.; Carr, A. J.; Daniels, S. M.; Gleeson, M. R.; Kelly, J. V.; Lawrence, J. R.; Sheridan, J. T. *J. Mater. Sci.* **2005**, *40*, 4129.
6. Lu, Y.; Chen, S. *Appl. Phys. Lett.* **2008**, *92*, 041109-1.
7. Burland, D; Bräuchle, C. *J. Chem. Phys.* **1982**, *76*, 4502.
8. Bräuchle, C.; Burland, D. *Angew. Chem. Int. Ed. Engl.* **1983**, *22*, 582.
9. Dorkenoo, K.; van Wonderen, A. J.; Bulou, H.; Romeo, M.; Crégut, O.; Fort, A. *Appl. Phys. Lett.* **2003**, *83*, 2474.
10. Hadis, M. A.; Tomlins, P. H.; Shortasll, A. C.; Palin, W. M. *Dent. Mater.* **2010**, *26*, 1106.
11. Dudi, O.; Grubbs, W. T. *J. Appl. Polym. Sci.* **1999**, *74*, 2133.
12. Fogleman, E. A.; Kelly, M. T.; Grubbs, W. T. *Dent. Mater.* **2002**, *18*, 324.
13. Inoue, K.; Komatsu, S.; Trinh, X. -A.; Norisuye, T.; Tran-Cong-Miyata, Q. *J. Polym. Sci. Part B: Polym. Phys.* **2005**, *43*, 2898.
14. Tran-Cong-Miyata, Q.; Van-Phem, D. -T.; Noma, K.; Norisuye, T.; Nakanishi, H. *Chin. J. Polym. Sci.* **2009**, *27*, 23.
15. Lam, J. F.; Tangonan, G. L. *IEEE Photon. Technol. Lett.* **1992**, *3*, 1102.
16. Jariwala, A.; Schwerzel, R. E.; Werve, M.; Rosen, D. W. In: Proceedings of the ASME 2012 International Symposium on Flexible Automation; St. Louis, MO; June 16–18, **2012**; Paper ISFA2012-7127.
17. Bennett, J. M. In: Handbook of Optics, 2nd Ed; Bass, M. Ed.; McGraw-Hill, Inc.: New York, **1995**; Vol.*1*, Chapter 5.
18. http://www.sartomer.com/wpapers/20551.pdf. Sartomer, Inc. product bulletin on SR351H, trimethylolpropane triacrylate; last accessed on 15 June 2011.
19. Monroe, B.; Weed, G. C. *Chem. Rev.* **1993**, *93*, 435.
20. Kaczmarek, H.; Galka, P. *Open Process Chem. J.* **2008**, *1*, 8.
21. Jariwala, A.; Schwerzel, R. E.; Rosen, D. W. *Proc. Solid Free-form Fabric. Symp.* **2011**, *22*, 99.